Title
Evaluation and optimization of a micro-tubular solid oxide fuel cell stack model including an integrated cooling system

Authors
Hering, Martin
Brouwer, Jacob
Winkler, Wolfgang

Publication Date
2016

DOI
10.1016/j.jpowsour.2015.09.036

Journal of Power Sources 303 (2016) 10–16

Contents lists available at ScienceDirect

Journal of Power Sources

journal homepage: www.elsevier.com/locate/jpowsour

Evaluation and optimization of a micro-tubular solid oxide fuel cell stack model including an integrated cooling system

Martin Hering [a], Jacob Brouwer [b, *], Wolfgang Winkler [a]

[a] Hamburg University of Applied Sciences, Berliner Tor 5, 20099, Hamburg, Germany
[b] National Fuel Cell Research Center, University of California, Irvine, CA, 92697, United States

HIGHLIGHTS

- Quasi three-dimensional, micro-tubular solid oxide fuel cell and stack model.
- Spatially resolved, transient thermodynamic, physical and electrical model.
- Model includes an integrated cooling system.
- Detailed parameter analysis of operating, geometrical and material properties.
- Optimization of the MT-SOFC stack based on results of parameter analysis.

ARTICLE INFO

Article history:
Received 31 March 2015
Accepted 8 September 2015
Available online 7 November 2015

Keywords:
Micro-tubular solid oxide fuel cell
MT-SOFC
Modeling
Integrated cooling system
Parameter analysis

ABSTRACT

A micro-tubular solid oxide fuel cell stack model including an integrated cooling system was developed using a quasi three-dimensional, spatially resolved, transient thermodynamic, physical and electrochemical model that accounts for the complex geometrical relations between the cells and cooling-tubes. For the purpose of model evaluation, reference operating, geometrical and material properties are determined. The reference stack design is composed of 3294 cells, with a diameter of 2 mm, and 61 cooling-tubes. The stack is operated at a power density of 300 mW/cm^2 and air is used as the cooling fluid inside the integrated cooling system. Regarding the performance, the reference design achieves an electrical stack efficiency of around 57% and a power output of 1.1 kW. The maximum occurring temperature of the positive electrode electrolyte negative electrode (PEN)-structure is 1369 K. As a result of a design of experiments, parameters of a best-case design are determined. The best-case design achieves a comparable power output of 1.1 kW with an electrical efficiency of 63% and a maximum occurring temperature of the PEN-structure of 1268 K. Nevertheless, the best-case design has an increased volume based on the higher diameter of 3 mm and increased spacing between the cells.

1. Introduction

Micro-tubular high temperature solid oxide fuel cells (MT-SOFCs) have advantages like high electrical efficiencies [1,2], long term stability [1,3], enhanced thermal cycling performance with rapid start-up and shut-down capabilities [1,3–5], high thermal shock resistance [4–6], high fuel flexibility [1,6], low emissions of carbon dioxide and criteria pollutants [1], the capability to be produced at low costs [3,7], as well as potential use in a variety of applications [6]. Thus, within the scope of worldwide energy challenges, MT-SOFCs are a promising energy conversion technology.

In our previous work a model of a novel anode-supported MT-SOFC stack design with the possibility of an integrated cooling loop was developed. In this concept, the stack can be internally cooled by thermal radiation. Thus, the air cooling demand can be reduced substantially. Therefore, auxiliary compressing power and exhaust gas losses are lowered. Regarding the setup inside the stack, metallic cone shaped interconnects link the anode of each cell with the cathode of the adjacent cells. Multiple levels of the bundled cells can be connected to form an entire stack design with the possibility to replace a cascade of cells with a heat exchanger tube to integrate a cooling system. A cooling fluid is circulated inside the heat exchanger tubes to reject the heat from the stack. This fluid

* Corresponding author.
E-mail address: jb@nfcrc.uci.edu (J. Brouwer).

http://dx.doi.org/10.1016/j.jpowsour.2015.09.036
0378-7753/

can be circulated in a closed loop if the heat is transferred to an external heat sink. This stack design is compact, light, and potentially robust with the ability to reject heat inside the stack due to the integrated cooling structure [1].

The chosen modeling approach is based upon a simplified tubular geometry and stack design. It includes detailed pressure drop and gas property calculations, as well as control strategies for the cell and stack temperature difference. Moreover, the electrical and physical constraints of the stack design are included to determine the stack current. Additionally, the implemented detailed radiative heat transfer between the cells and the integrated cooling-tubes, convective heat transfer between the gas flows and the surrounding structures and conductive heat transfer between the solid structures inside of the stack leads to an advanced heat transfer balance.

This quasi three-dimensional, spatially resolved, transient thermodynamic, physical and electrochemical micro-tubular solid oxide fuel cell and stack model including an integrated cooling system was implemented in the MatLab Simulink environment, as an extension of the planar SOFC model by McLarty et al. [8–10]. The model only simulates a vertical cross section of the stack, which is divided into rows and columns. The column accounts for the number of cascading cells, while the number of rows represents the number of parallel cascades of cells in the cross section.

Each row–column combination contains a module, which is comprised of 6 cells and a cooling-tube. Thus, on each stack layer or column only modules in a straight line regarding the cross-flow air stream are simulated. However, the equations are only solved for a single cell of a module, since an analogous performance is assumed. Additionally, the results of a single cross section through the entire stack in the air flow direction is assumed to represent all adjacent cross-sections of the stack. In conclusion, the thermal interactions between the cells and the cooling-tubes can be modeled in every module without the need of an extension to a complete three-dimensional model. A top view of the previous described cross section with 6 rows and the highlighted module setup is illustrated in Fig. 1.

In this work the previously described MT-SOFC stack model is evaluated with the help of a parametric variation analysis. Furthermore, the results of the parameter variations are used to determine a best-case design.

2. Model evaluation approach

For the purpose of model evaluation, reference operating, geometrical and material properties, as well as evaluating ranges for the entire stack design are determined based upon a literature review regarding micro-tubular solid oxide fuel cells [11], the results of the previous conducted related research [12] and a simplified preliminary evaluation of the modeling approach. The literature review outlined that one of the major used material sets of MT-SOFCs is comprised of a Ni-YSZ (nickel, yttria-stabilized zirconia) anode, a YSZ electrolyte and an LSM (lanthanum strontium manganite) cathode. Those cells are mainly operated in a temperature range between around 773 to 1173 K. Therefore, the parametric variations in temperature levels at the stack inlet and outlet are chosen to match this literature temperature level. Moreover, the power density range is also determined based upon the literature studies resulting large range of current density levels. It is also assumed that it is possible to run the MT-SOFC stack on pure humidified methane. The designated reference properties and the designated evaluated ranges of each selected parameter for the parameter analysis are shown in Table 1.

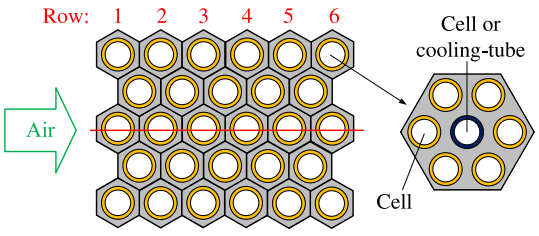

Fig. 1. Top view of model structure with module design.

The pressure ratio determines the outlet pressure based on the ambient pressure, as shown in Eq. (1). Therefore, the absolute pressure level of the stack is defined by the pressure ratio since the inlet pressure is calculated backwards based upon the outlet pressure and the calculated pressure drops through the stack.

$$\delta_p = \frac{p_{out,F/Air/CF}}{p_{amb}} \tag{1}$$

The fuel used is assumed to be pure methane. For the calculation of different inlet fuel composition it is assumed that a portion of the used methane is pre-reformed to produce an equilibrium composition associated with steam methane reforming and water gas shift reactions expressed by the pre-reforming percentage of methane, X.

For a simplified system approach, the parasitic power demand of the fuel, air and cooling fluid blowers are estimated based upon the calculated pressure drops and designated blower efficiencies. A simplified system net power output is calculated using the parasitic power demand of the blowers to estimate the influence of the pressure drops on the system performance. Therefore, the system efficiency is expressed as the net power output divided by the lower heating value of methane, as illustrated in Eq. (2). The stack efficiency is related to the gross power output of the stack, the fuel composition at the associated inlet and the corresponding lower heating values of the burnable species.

$$\eta_{Sys} = \frac{P_{el,S} - \sum P_{Blower,el,F/Air/CF}}{\dot{n}_{CH_4,Sys,inl}\, LHV_{CH_4}} \tag{2}$$

To account for the influence of a reformer in a system with pre-reforming of methane, the system efficiency is additionally lowered by a reformer efficiency, as shown in Eq. (3). The reformer efficiency for a certain pre-reforming percentage of methane is scaled based upon the increase of the molar flow rate of fuel at the stack inlet and the total spread between the assumed reformer efficiencies, as well as the total molar flow rates of a system with pre-reforming percentages of methane of 0 and 1, as illustrated in Eq. (4). It is assumed that the losses in a system with a pre-reforming percentages of methane of 100% are in the order of 10%. Thus, the reformer efficiency is scaled between 90% and 100% for a system with complete and without pre-reforming.

$$n_{Sys,Reformer} = n_{Sys}\, \eta_{Reformer} \tag{3}$$

$$\eta_{Reformer} = 1 - \frac{1 - \eta_{Reformer,X=1}}{\dot{n}_{X=0} - \dot{n}_{X=1}} \sum_{k=1}^{10X} \dot{n}_{k-1} - \dot{n}_k \tag{4}$$

The compactness of a stack design is evaluated using the power density related to the total stack volume and power output, as shown in Eq. (5).

$$p_{V,S} = \frac{P_{el,S}}{V_S} \tag{5}$$

Table 1
Operating, geometry and material properties for the reference and best-case design.

Operating properties	Reference	Evaluation	Best-case
Power density – p_A in mW cm^{-2}	300	50–550	300
Type of cooling fluid	Air	He/Ar/N_2	Ar
Stack cooling operation	ICS	ACS	ICS
Cooling fluid flow direction	Counter-flow	Co-flow	Counter-flow
Inlet fuel temperature – $T_{F,inl}$ in K	1023	923–1123	1123
Inlet air temperature – $T_{Air,inl}$ in K	1023	923–1123	1048
Inlet cooling fluid temperature – $T_{CF,inl}$ in K	773	573–973	973
Limiting temperature spread – ΔT in K	150	50–200	70
Air utilization factor – U_a	0.4	0.2–0.7	0.3
Fuel utilization factor – U_f	0.85	0.70–0.90	0.90
Steam-to-carbon-ratio – S/C	2	1.5–3.0	1.5
Pre-reforming percentage of methane – X	0	0–1	0
Pressure ratio – δ_p	1	1–2	1
Estimated blower efficiency – η_{Blower}	0.8	0.15–0.95	0.95
Geometry and material properties	**Reference**	**Evaluation**	**Best-case**
Number of columns – N_{column}	9	3–11	9
Number of rows – N_{row}	9	3–11	9
Stack layer design option	Shell	Square	Sqaure
Outer diameter of a cell – $d_{C,o}$ in mm	2	1–5	3
Cell diameter to spacing ratio – $\delta_{d/s}$	2	0.25–3.75	1.5
Thickness of anode in μm	200	–	200
Thickness of cathode in μm	50	–	50
Thickness of electrolyte in μm	25	–	25
Thickness of anode/cathode interconnect in mm	0.2	–	0.2
Length of a single cell – l_C in mm	20	10–50	10
Cell length to interconnect height ratio – $\delta_{l/h}$	10	4–20	20
Height of interconnect layer – h_{Inter} in mm	0.2	–	0.2
Thickness of a cooling-tube in μm	150	–	150
Height of the spacer – h_{Sp} in mm	0.2	–	0.2
Emissivity of the cell – ε_C	0.30	0.10–0.90	0.40
Emissivity of the cooling-tube – ε_{CT}	0.85	0.10–0.90	0.40

Ensuing from the designated reference design, a parametric variation analysis is conducted to estimate the impact of each individual evaluated parameter on the performance and compactness of the stack. The analysis includes the variation of the temperature and pressure levels, fuel and air utilization factors, inlet fuel compositions, cooling fluid type and flow directions, power densities, assumed blower efficiencies, design options of the stack, cell diameters and lengths, spacing between two cells, interconnect lengths, as well as materials properties. The designated evaluated ranges of each parameter for the analysis are shown in Table 1. In this evaluation only a single parameter is varied in a chosen range, while all others are kept at their designated reference value. Moreover, as a result, parameters of a best-case design are determined based upon the combined evaluation of the single factor analysis. The best-case parameters are chosen on the basis of maximizing the system efficiency in each individual category.

3. Results

3.1. Reference evaluation

For the reference evaluation 81 cells, arranged in 9 rows and columns, are simulated. Therefore, the stack design is composed of 3294 cells with an outer diameter of 2 mm and 61 cooling-tubes. It achieves an electrical efficiency of around 57% and a power output of 1.1 kW. The volume of the stack is around 0.65 dm^3. Therefore, the stack has an electrical power density based on the total volume of the stack of 1.7 W/cm^3. A scaled three-dimensional drawing of the reference design is illustrated in Fig. 2a. The major geometrical features and calculated performance results of the reference stack design operated on the designated reference parameters are shown in Table 2.

The general flow directions of the fuel, air and cooling fluid stream, as well as the segmentation of the stack design in rows and columns is simplified shown for 1 row and 2 columns in a cross-section in Fig. 3. As previously mentioned, every simulated cell in a single row–column combination represents a module containing 6 cells and a single cooling-tube. As shown in Fig. 4a, the resulting temperature profile of the reference case exhibits a cone shape with its temperature maximum in the upper central portion of the stack. The first column of the stack has the lowest temperature since most of the internal steam reforming is occurring at the fuel inlet. The

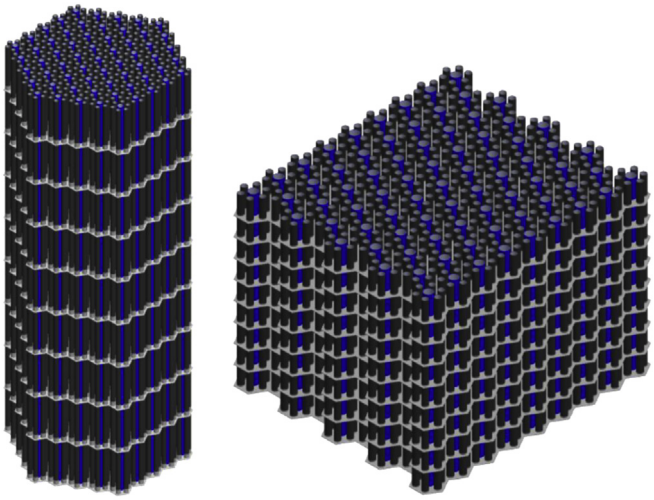

Fig. 2. Three-dimensional drawing of the reference (a) and best-case design (b) – Scale ~ 1:3.

Table 2
Data of reference and best-case evaluation.

Parameter	Reference	Best-case
Number of cells – $N_{C,S}$	3294	4158
Number of cooling-tubes – $N_{CT,S}$	61	77
Current per stack layer – I_{SL} in A	4.373	3.319
Stack power output – $P_{el,S}$ in kW	1.118	1.117
System power output – $P_{el,Sys}$ in kW	1.114	1.115
Stack electrical efficiency – $\eta_{el,S}$	0.571	0.630
System efficiency – $\eta_{el,Sys}$	0.569	0.630
Pressure drop air side – Δp_{Air} in kPA	1.411	0.621
Pressure drop fuel side – Δp_F in kPA	2.017	0.085
Pressure drop cooling fluid side – Δp_{CF} in kPA	1.235	0.095
Total volume of the stack – V_S in dm^3	0.645	1.142
Volumetric power density – $p_{V,S}$ in W cm^{-3}	1.732	0.978
Maximal PEN temperature – $T_{PEN,max}$ in K	1369.217	1267.550
Maximal temperature spread of cell – $\Delta T_{C,max}$ in K	88.355	45.313

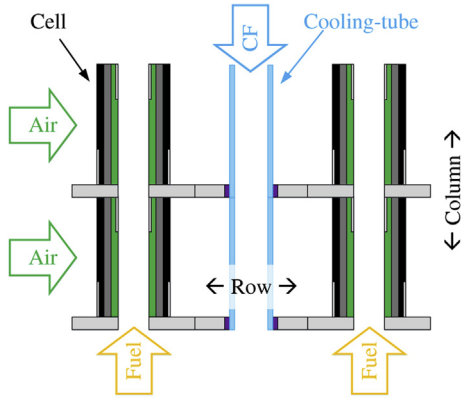

Fig. 3. Flow directions and segmentation of the stack design.

cone shape in the central portion of the stack is a result of the increased air and cooling fluid temperatures in this region of the stack. The air and cooling fluid are constantly heated as they flow through the stack, while the cooling effect of the internal methane steam reforming is vanishing in the direction of the fuel stream flow since the methane tends to react completely near the fuel inlet on the first columns. Hydrogen is not depleted uniformly throughout the stack since the cone shaped temperature profile in combination with the applied physical constraints leads to a current or power density distribution as shown in Fig. 4b. As illustrated, the highest power densities occur in the front central portion of the stack. Therefore, hydrogen is depleted faster in the first rows of the stack. This effect causes the changing power density distribution in the upper portion of the stack since the hydrogen content in the first rows is too low to sustain a strong electrochemical conversion. Thus, more hydrogen is converted in the upper middle and end portion of the stack directly correlated with the higher cell currents. However, the low hydrogen content in the upper first rows of the stack leads to an enhanced formation of carbon dioxide since the water gas shift equilibrium reaction is shifting to the product side. This strong shift is based on Le Chatelier's principle as water vapor is formed and hydrogen is depleted to very low mole fractions due to the electrochemical conversion. Additionally, the low hydrogen content in these regions of the stack are also visible in the distribution of the fuel utilization factor of each individual cell, as illustrated in Fig. 4c. Based on the applied physical current and voltage constraints and the resulting temperature profile, high fuel utilization factors per cell of nearly 0.6 occur in the top left portion of the stack. The evaluation of the reference parameters clarifies that the chosen modeling approach

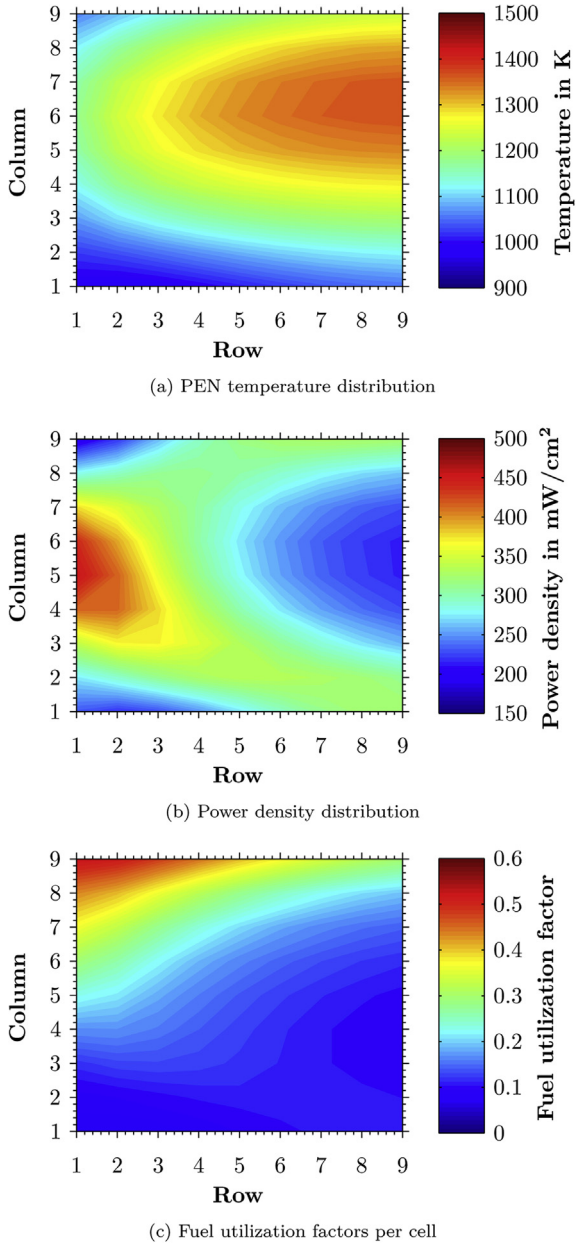

(a) PEN temperature distribution

(b) Power density distribution

(c) Fuel utilization factors per cell

Fig. 4. Reference design results.

with the applied physical constraints and controllers allows a detailed analysis of a micro-tubular stack design with an integrated cooling structure. The model evaluation accounts for the complex geometrical relations and achieves explainable and consistent results.

3.2. Parameter analysis

As previously mentioned, the designated evaluated ranges of each parameter for the analysis are shown in Table 1. As a result, parameters of a best-case design are determined based upon the combined evaluation of the single factor analysis. However, the best-case results are already briefly shown in the parameter analysis, while the detailed evaluated of the best-case design is presented in subsection 3.3.

The result of the parameter analysis, regarding the deviation of the electrical system efficiency for each evaluated parameter as a

percentage of the reference, is shown in Fig. 5a. In comparison to a system running on pure air cooling without an integrated cooling system (ACS), the reference design achieves an efficiency increase of around 1%. Except for the fuel utilization factor U_f, the positive impact of all parameter variations on system efficiency is less than 2.5%. However, the analysis of the fuel utilization factor clarified that very high fuel utilization factors of the stack can lead to excessively high fuel utilization factors in single cells in the end portion of the stack. Those high fuel utilization factors can lead to carbon deposition and faster cell degradation that limit the practical range of fuel utilization. In the best-case design the overall fuel utilization factor was selected to be 0.9, with the resulting highest per cell utilization factors of around 0.6. Note that the best-case design achieves a 10.7% increased system efficiency compared to the reference design. Regarding the parameters that had a negative impact on system efficiency compared to the reference system efficiency, especially the co-flow operation, fuel and air utilization factor U_a, pre-reforming percentage of methane X and pressure ratio δ_p can lead to a significant decrease of more than 5%. In a co-flow operation the stack inlet gets excessively cooled by the cooling fluid flow and the occurring steam methane reforming. Therefore, the voltage levels and thus the efficiencies are notably lower. A lower fuel utilization factor leads to a reduced efficiency since the portion of unused fuel in the anode exhaust is increasing. High air utilization factors cause non uniform temperature profiles which lead to lower voltage levels and efficiencies. Higher pressure ratios excessively increase the parasitic blower power demand and therefore significantly decrease efficiencies. As a result of the high cooling fluid demands, high pre-reforming percentages of methane cause low voltage levels on the last stack layers and thus reduced efficiencies. Nevertheless, a certain pre-reforming percentage of methane around 0.4 leads to an enhancement of the system efficiency due to a preferred and more uniform temperature distribution inside the stack. The analysis clarified, that the impact on system efficiency of the used cooling fluid *He*, N_2 or *Ar*, the emissivities of the cells and cooling-tubes $\varepsilon_{C|CT}$, the ratio between the length of a cell and the height of an interconnect $\delta_{l/h}$, as well as the use of a square or shell stack layer design are very low. The system efficiency of the reference design is only moderately influenced on both sides by the change of the inlet temperature of air T_{Air}, fuel T_F or the cooling fluid T_{CF}, the temperature spread ΔT, the outer diameter $d_{C,o}$ and length l_C of a cell, as well as the spacing to diameter ratio $\delta_{d/s}$.

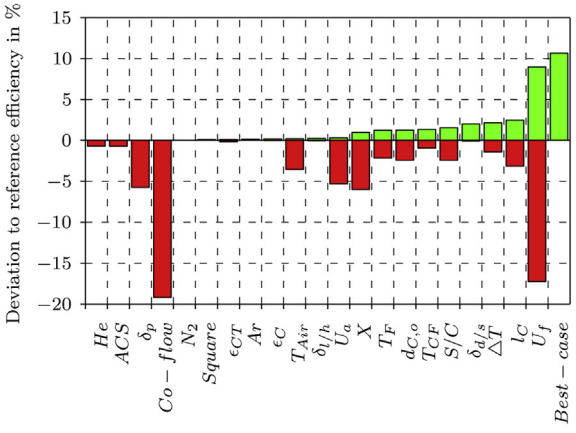

(a) Deviation of system efficiencies

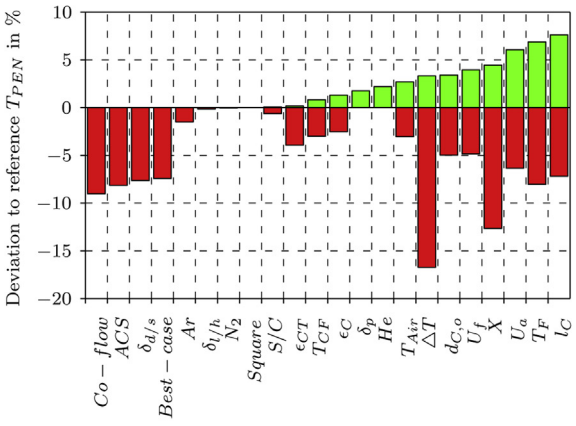

(b) Deviation of PEN temperatures

Fig. 5. Deviation of system efficiencies and PEN temperatures of each evaluated parameter and best-case design to the reference design.

Besides the electrical system efficiency, another important output is the maximum occurring temperature of the PEN-structure since it is possible that some design and operating conditions could lead to excessively high values due to the temperature distribution in a design with an integrated cooling system. In the reference design the maximum occurring temperature of the PEN-structure is 1369 K, which is too high. The impact of all parametric variations upon the maximum occurring PEN temperatures as a percentage of the reference, is shown in Fig. 5b. Especially, the temperature spread, the pre-reforming percentage of methane, the cooling fluid temperature, the air utilization factor, the ratio between the diameter and spacing, the outer diameter and length of a cell, as well as the emissivities of a cell and a cooling-tube are able to reduce the maximum occurring PEN temperature by up to 17% without harming the electrical efficiency. In all these cases, the resulting temperature profile is more uniform and causes an enhanced total voltage level, especially on the first stack layers. The inlet temperatures of the air and fuel, the steam-to-carbon-ratio, the fuel utilization factor, the pressure ratio and a co-flow operation are also able to reduce the maximum occurring PEN temperature. Nevertheless, in those cases a reduction of the temperature is always connected with a corresponding decrease of the system efficiency due an overall lower voltage level. Despite the steam-to-carbon ratio, the lower voltage levels are a result of excessive cooling at the stack inlet. In case of the steam-to-carbon ratio, the reduced voltage is based upon the decreased Nernst voltage due to higher mole fraction of water in the fuel. In total, the adjustment of the parameters in the best-case design leads to a reduction of the maximum occurring PEN temperature by 7.4%, leading to a maximum occurring PEN temperature of 1268 K. Moreover, the best-case design achieves a comparable power output to the reference design of 1.1 kW with an electrical efficiency of 63%. Nevertheless, the best-case design is less compact due to the higher outer cell diameter of 3 mm and additional spacing between the cells.

In brief, the evaluation of the modeling approach clarifies that even small changes of single parameters can have significant impacts on the performance and compactness of the stack design. Moreover, by varying multiple factors at once, it is possible to combine a plurality of positive effects to improve the efficiency and temperature distribution as was shown with the best-case design. Note that the evaluated best-case design may not be the design with the maximum efficiency since the parameters were chosen based upon the results of the single factor parameter analysis. Application of a formal optimization technique to the current model could produce a stack design and operating conditions that are superior to the best-case design presented here. In the next subsection a detailed evaluation of the best-case design is

presented.

3.3. Best-case evaluation

As mentioned previously, the best-case parameters are chosen based on the results of the analysis of each evaluated parameter on the basis of maximizing the electrical system efficiency for each of the single parameter variations. Therefore, the best case parameters are determined based upon the system efficiency maximum associated with the variation of each parameter. Compared to the reference operating properties, the inlet temperature of the fuel, air and cooling fluid, the fuel utilization factor and the blower efficiency are increased. The integrated cooling system is operated on argon in a counter-flow operation. The air utilization factor, steam-to-carbon-ratio and temperature spread are lowered. The designated power density, pre-reforming percentage of methane and the pressure ratio are kept constant to operate on comparable gas composition, reformation rates and fuel consumption. Regarding the geometry and material properties, a square design with 9 rows and 9 columns is chosen to compare designs with equal power outputs. The cell diameter, the diameter to spacing ratio and the length of a cell are lowered, while the ratio between the length of a cell and the height of an interconnect is increased. All other geometrical parameters are kept constant. The emissivities of either a cell or a cooling-tube are set to intermediate values. The comparison of the operating, geometrical and material properties of the reference and best-case design is shown in Table 1. Additionally, a scaled three-dimensional drawing of the best-case design is illustrated in Fig. 2b.

As shown in Table 2, the resulting best-case design has a higher number of cells and cooling-tubes since the square stack layer design is used. However, the stack and system power output is nearly equal since the cells in the best-case design are only half as long. Thus, the active surface area per single cell is smaller. Nevertheless, the current per stack layer is lower and the cell voltages are higher. Therefore, the stack and system efficiency are both around 6% points higher for the best-case design. The pressure drops on the fuel, air and cooling fluid side in the best-case design are significantly lower because of the enlarged channel sizes. Additionally, as illustrated in Fig. 6a, in the best-case design the temperature distribution is more uniform and the maximal occurring PEN temperature, as well as the temperature spread per single cell is remarkably lower. The reduced temperature differences result from a combination of the lower air utilization factor, the decreased limiting temperature spread and changing view factors due to bigger diameters and spacings between cells and cooling-tubes. Moreover, the increased uniformity of the temperature distribution leads to a more uniform power density distribution, as shown in Fig. 6b. The more uniform power density distribution also leads to an enhanced uniformity of the distribution of the fuel utilization factors of the cells on a single stack layer, as illustrated in Fig. 6c. Nevertheless, the fuel utilization factors per single cell on the last stack layer are very high since the total fuel utilization factor is increased compared to the reference case. On the downside, the volume of the best-case stack design is nearly doubled and thus the volumetric power density is remarkably lower since the diameter of the cells, as well as the spacing between two cells is higher. Additionally, comparing the reference and best-case design over the entire power density range shows a gap of around 6% points between the reference and best-case efficiencies throughout the range considered. The increased efficiency is due to two major factors. Firstly, the voltage levels on the first and second stack layer are remarkably higher for the best-case. This increase is based on the higher average temperatures and thus reduced ohmic losses in this region for the best-case. Secondly, the parasitic blower

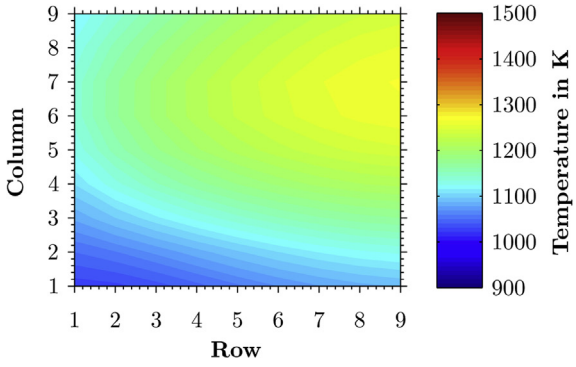

(a) PEN temperature distribution

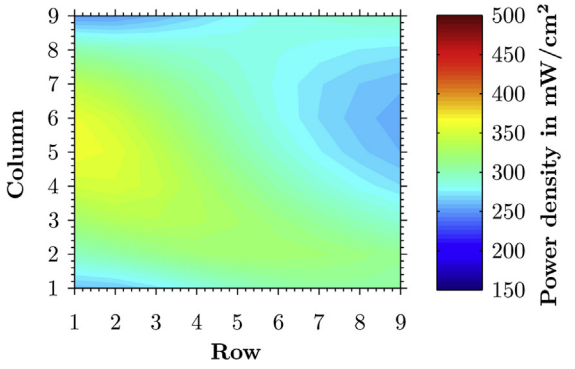

(b) Power density distribution

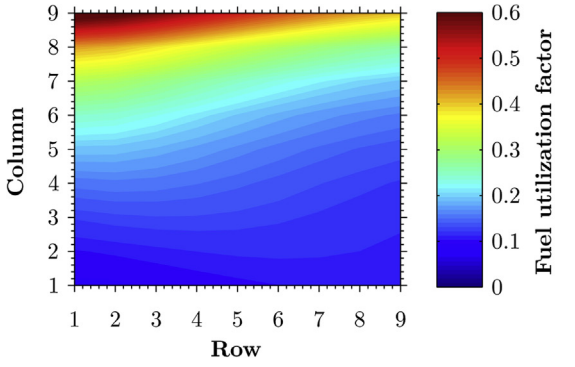

(c) Fuel utilization factors per cell

Fig. 6. Best-case design results.

demands are lower in the best-case design since the pressure drops are significantly reduced.

4. Conclusion

A quasi three-dimensional, spatially resolved, transient thermodynamic, physical and electrochemical micro-tubular solid oxide fuel cell and stack model including an integrated cooling system was evaluated and optimized. The modeling approach was evaluated by defining reference parameters and corresponding evaluating ranges of each parameter. The reference design has an outer cell diameter of 2 mm achieves an electrical stack efficiency of around 57% and a power output of 1.1 kW with a maximum PEN temperature of 1369 K. Stack design and operating conditions were systematically varied to estimate the impact of each individual parameter on the performance of the stack. Moreover, a best-case design was determined based upon maximizing the system

efficiency for each parametric variation. The best-case design has an outer cell diameter of 3 mm and achieves a comparable power output of 1.1 kW with an electrical efficiency of 63% and a maximum occurring temperature of the PEN-structure of 1268 K.

Acknowledgments

We gratefully acknowledge the support of Dustin Fogle McLarty, Ph.D. in the model development process.

References

[1] G. Tsotridis, Micro-tubular Solid Oxide Fuel Cell Arrangement, 2012. US Patent App. 14/119,249.
[2] V. Lawlor, J. Power Sources 240 (2013) 421–441.
[3] C. Chen, M. Liu, L. Yang, M. Liu, Int. J. Hydrogen Energy 36 (2011) 5604–5610.
[4] F. Calise, G. Restucccia, N. Sammes, J. Power Sources 195 (2010) 1163–1170.
[5] N. Akhtar, S. Decent, D. Loghin, K. Kendall, J. Power Sources 193 (2009) 39–48.
[6] V. Lawlor, S. Griesser, G. Buchinger, A. Olabi, S. Cordiner, D. Meissner, J. Power Sources 193 (2009) 387–399.
[7] W. Winkler, Brennstoffzellenanlagen, Springer, 2002.
[8] D. McLarty, J. Brouwer, S. Samuelsen, Int. J. Hydrogen Energy 38 (2013) 7935–7946.
[9] D.F. McLarty, Fuel Cell Gas Turbine Hybrid Design, Control, and Performance, University of California, Irvine, 2010.
[10] D.F. McLarty, Thermodynamic Modeling and Dispatch of Distributed Energy Technologies Including Fuel Cell–Gas Turbine Hybrids, University of California, Irvine, 2013.
[11] N. Kamran, M. Hering, Dimensioning of an SOFC-Stirling System - Literature Research and Modeling of SOFC-Stirling Hybrids, Hamburg University of Applied Sciences, 2014.
[12] M. Hering, Dimensioning of an SOFC-Stirling System - Conception of the SOFC Stack, Hamburg University of Applied Sciences, 2014.

Nomenclature

List of Latin symbols

d: Diameter in m
h: Height in m
I: Current in A
l: Length in m
LHV: Lower heating value in J mol^{-1}
N: Number
P: Power in W
p: Pressure in Pa
p_A: Areal electrical power density in W m^{-2}
p_V: Volumetric electrical power density in W m^{-3}
S/C: Steam-to-carbon-ratio
T: Thermodynamic temperature in K
U_a: Air utilization factor
U_f: Fuel utilization factor
V: Volume in m^3
X: Pre-reforming percentage of methane

List of Greek symbols

δ: Ratio
η: Efficiency
Δ: Change of quantity
ε: Emissivity

List of subscripts

amb: Ambient
C: Cell
CF: Cooling fluid
CH_4: Methane
CT: Cooling-tube
d/s: Diameter to spacing
el: Electric
F: Fuel
inl: Inlet
Inter: Interconnect
k: Running index
l/h: Length to height
max: Maximal
o: Outer
out: Outlet
p: Pressure
PEN: Positive electrode electrolyte negative electrode
S: Stack
SL: Stack layer
Sp: Spacer
Sys: System

List of abbreviations

ACS: Air cooled system
CF: Cooling fluid
LSM: Lanthanum strontium manganite
MT: Micro-tubular
Ni: Nickel
PEN: Positive electrode electrolyte negative electrode
SOFC: Solid oxide fuel cell
YSZ: Yttria-stabilized zirconia